ADVANCED MATERIALS
www.advmat.de

Relationship between Crystalline Order and Exciton Diffusion Length in Molecular Organic Semiconductors

By *Richard R. Lunt, Jay B. Benziger,* and *Stephen R. Forrest**

One of the most fundamental properties of both organic and inorganic semiconductors is charge mobility. It has been unambiguously shown that the mobility in both of these materials systems is strongly linked to the degree of long range order—that is, more extended crystallinity leads to a larger charge mobility, which ultimately determines such extrinsic properties as series resistance and response to current and optical pulses. An equally fundamental property for organic semiconductors is the molecular excited state-, or exciton-, diffusion length which characterizes energy transport within these more correlated solids. While it has been predicted that exciton transport should also be linked to the extent of crystalline order, to our knowledge no such dependence has yet been established. Here, we accurately measure the exciton diffusion length of the archetypal organic semiconductor, 3,4,9,10-perylenetetracarboxylic dianhydride (PTCDA) and clearly show its relationship to thin-film crystal morphology. As in the case of charge mobility, we show that the exciton transport diffusion length is a monotonic function of the extent of crystalline order. This study provides insight into the control and ultimately the tunability of the exciton diffusion length in organic systems, which is crucial for the management of energy transport in a wide range of important organic electronic devices.

The exciton diffusion length (L_D) and charge mobility in organic semiconductors are central parameters for the optimal design of organic thin film electronic devices.[1–4] For example, charge mobility, and hence material conductivity, can vary by several orders of magnitude depending on the degree of crystalline order,[5–7] where the largest values have been found for single crystals.[5,8] Analogously, exciton diffusion has also been suggested to depend on structural order.[9–12] For example, the triplet exciton transfer rate may be described by the product of electron and hole transfer rates[12] which connects the diffusion of excitons to charge carrier mobility. Yet, the correlation between L_D and crystalline order remain ambiguous. While the triplet diffusivities of amorphous[13] and crystalline[14–17] tetracene have been measured, no *systematic* dependence on crystallinity has been observed (i.e., reported values of exciton diffusivity in amorphous tetracene are both greater than and less than that of a single crystal). Other studies have explored possible connections between crystalline order and the exciton diffusion length in substituted phthalocyanines,[10,18] porphyrins,[18] perylene derivatives,[9,19] and polymers.[20] However, it is unclear from these studies whether the variations in the exciton diffusion length stem primarily from changes in the crystalline texture, the different electronic couplings of the various molecules, or from energetic disorder-induced transport percolation pathways.[21] Thus, despite the measurement of the exciton diffusion length for a large range of materials,[2,22–25] no clear functional dependence between the diffusion length and the degree of crystalline ordering has been demonstrated.

Here, we accurately measure the exciton diffusion length of PTCDA as a function of crystalline order using spectrally resolved photoluminescence quenching (SR-PLQ). Exciton diffusion is primarily attributed to Förster-assisted migration that monotonically increases with crystal size. Fitting these morphology-dependent trends with a simple model for the nonradiative rate of excitons in the solid, we show that the room temperature diffusion length asymptotes to that of a single crystal for grain sizes exceeding approximately $20 \cdot (L_D$ of single crystals).

The extent of crystalline order of PTCDA thin films was varied using a range of vapor phase growth conditions, in combination with structural templating on (100) KBr substrate surfaces (see Experimental). Accurate measurement of the diffusion length as a function of growth conditions (and hence the extent of crystalline order) were performed using SR-PLQ, with results summarized in Figure 1. The magnitude of photoluminescence quenching (η) of thick PTCDA samples coated with exciton blocking and quenching layers is related to the exciton generation profile determined by the absorption coefficient (α). The η–α data are then fit with a diffusion model to extract the diffusion length.

The corresponding grain size and crystal orientation were probed with a combination of atomic force microscopy (AFM), cross-sectional scanning electron microscopy (SEM), and X-ray diffraction (XRD). Atomic force microscopy scans of the surface morphologies of several films are provided in Figure 2a, with cross-sectional SEM images in Figure 2b clearly showing the grain boundaries for the case of $L_D = 9.5$ nm (left image) and 21.5 nm (right image). In general, L_D increases with the grain size (as determined from AFM analysis), which is found to increase with growth temperature. For example, the diffusion length increases from 6.5 ± 1.0 nm in the amorphous limit (where the average grain size is $\langle R \rangle = 0 \pm 5$ nm), to 21.5 ± 2.5 nm for large grain crystalline films ($\langle R \rangle = 400$ nm) along the (102) PTCDA direction. Corresponding XRD data in Figure 3a exhibit two diffraction peaks attributable to flat-lying α-PTCDA, (indexed as

[*] Prof. S. R. Forrest, R. R. Lunt
Department of Physics, Electrical Engineering and Computer Science
University of Michigan, Ann Arbor, Michigan 48109 (USA)
E-mail: stevefor@umich.edu
Prof. S. R. Forrest, R. R. Lunt
Department of Materials Science and Engineering
University of Michigan, Ann Arbor, Michigan 48109 (USA)
R. R. Lunt, Prof. J. B. Benziger
Department of Chemical Engineering
Princeton University, Princeton, NJ 08544 (USA)

DOI: 10.1002/adma.200902827

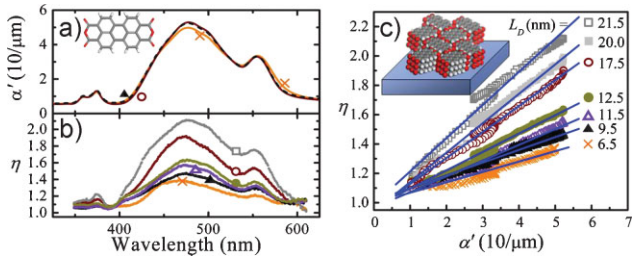

Figure 1. Measurement of PTCDA diffusion length using spectrally resolved photoluminescence quenching. a) Measured absorption coefficients corrected for non-normal incidence (α') for samples grown under a variety of conditions that vary the extent of crystalline order. Inset: chemical structure of PTCDA (C = gray, O = black, H = white). Degree of luminescence quenching (η) (see Experimental) versus b) wavelength and c) α'. Little variation in α' was observed over the range of growth conditions investigated. The quenching data were fit to the equation $\eta = \alpha' L_D + 1$ with the fitted diffusion length included for each curve in (c). Inset: crystal structure diagram of α-PTCDA oriented with the (102) plane parallel to the substrate surface. The symbols correspond to different substrate temperatures used during growth: T_{sub} = 440 (□), 435 (■), 430 (○), 420 (●), 395 (△), 295 (▲), 295 (no symbol, green), and 77 K (×). The latter two samples were grown with a thin (0.5 nm) templating layer of Ag to disrupt crystalline ordering. All the samples were grown on KBr substrates via vacuum thermal evaporation, except the sample grown at 77 K, which was grown by organic vapor phase deposition.

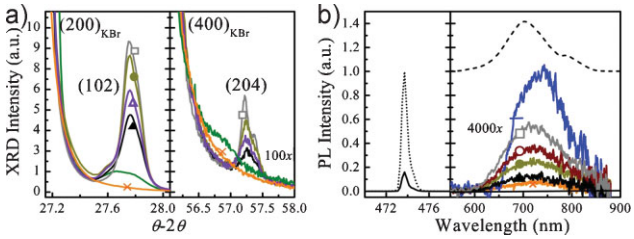

Figure 3. a) X-ray diffraction patterns of the 350 nm thick PTCDA films grown under various conditions, on single-crystalline KBr surfaces. The (102) and (204) PTCDA peaks are observed for all samples except the amorphous film (×). The (200) and (400) reflections of the KBr substrate appear as sharp shoulders. b) Photoluminescence quantum yield. The exciting laser spectrum is shown (left) with a bare substrate (dotted line, I_B^L) and with a PTCDA film (solid line, I_F^L) centered around a wavelength of 474 nm. Photoluminescence emission from the PTCDA films (right) in the integrating sphere (I_{Em}) and spectrofluorometer (dashed line) are shown. The symbols correspond to different substrate temperatures used during growth: T_{sub} = 440 (□), 435 (■), 430 (○), 420 (●), 395 (△), and 295 (▲), single crystal (—), 295 (green), and 77 K (×). The latter two samples were grown with a thin (0.5 nm) templating layer of Ag to disrupt crystalline ordering. All the samples were grown on KBr substrates via vacuum thermal evaporation, except the sample grown at 77 K, which was grown by organic vapor phase deposition.

the (102) and (204) planes) as shown inset in Figure 1c. The XRD data also show characteristic narrowing of the peak width (up to the measurement resolution of the system) with increasing in-plane grain size, indicating a concomitant increase in ordering of the crystal stacks parallel to the substrate normal. This suggests that grains increase in size in all three dimensions with the growth temperature.

To further understand the trends of exciton diffusion length in PTCDA, we consider the weak dipole–dipole coupling limit, where strong exciton–phonon interactions result in random hopping of excitons. In this case, Förster-mediated hopping is used to describe singlet exciton diffusion via:[22]

$$L_D = \sqrt{\frac{\kappa^2 \Phi_F}{8\pi n^4}\frac{\sigma}{a^4}} = \sqrt{\frac{\Phi_F}{6}}\frac{R_{00}^3}{a^2} \quad (1)$$

where κ is the dipole orientation factor,[22,26] n is the refractive index, σ is the Förster overlap integral,[26,27] $\Phi_F^{1/6} R_{00} = R_0$ is the Förster radius, and a is the average hopping distance.[28] The fluorescence quantum yield is $\Phi_F = k_r/(k_r + k_{nr} + \gamma) = k_r\tau$, where k_r is the radiative rate ($k_r = 3 \times 10^6\ s^{-1}$ for PTCDA[22]), k_{nr} is the nonradiative rate, and γ is the rate of excitation loss through other mechanisms (e.g., annihilation, fission, or intersystem crossing). For polycrystalline films with randomly oriented grains, L_D represents a spatial average. The nonradiative rate can be written as a sum of the component losses as:

$$k_{nr} = k_{nr}^0 + S_r P_G \quad (2)$$

where k_{nr}^0 is nonradiative rate in the single-crystal limit (including the rate of concentration quenching), S_r is the average nonradiative surface recombination rate for excitons at grain boundaries, and P_G is the probability of an exciton encountering a grain boundary. Assuming isotropic diffusion, we can approximate $P_G = L_D^3/\langle R \rangle^3$. Except at very high

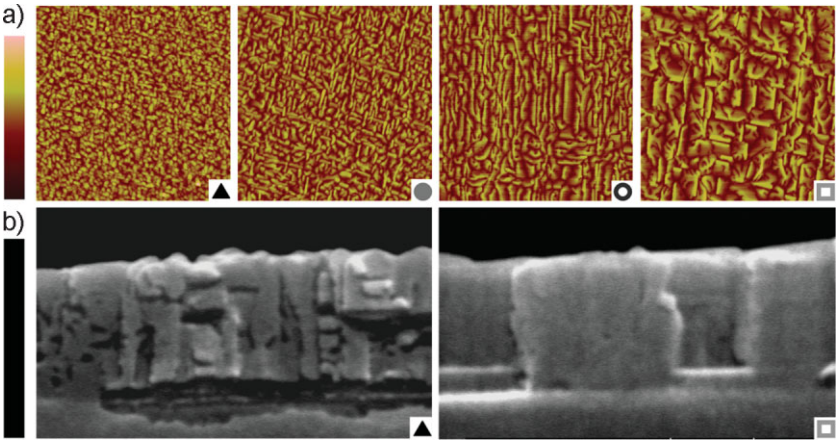

Figure 2. a) AFM images of thin (350 nm) PTCDA films grown under various conditions. The image widths and heights are 5 μm and 50 nm respectively. The root-mean-square surface roughness values from left to right are 7.0, 7.6, 8.0, and 8.2 nm. b) Cross-sectional SEM images of the PTCDA films (left and right SEM image correspond to the left- and right-most AFM images, respectively). The scale bar corresponds to 500 nm. The images show the polycrystallite dimensions corresponding to the texture observed in the AFM scans. The films are relatively flat despite varying grain sizes. The symbols correspond to different substrate temperatures used during growth: T_{sub} = 440 (□), 430 (○), 420 (●), and 295 K (▲).

intensities, γ is negligible in PTCDA,[29] and hence, the Förster-assisted diffusion length becomes:

$$L_D = \frac{R_{00}^3}{\sqrt{6}\cdot a^2}\sqrt{\frac{1}{1+K_1+K_2\left(\frac{L_D}{\langle R\rangle}\right)^3}} \quad (3)$$

where $K_1 = k_{nr}^0/k_r$ and $K_2 = S_r/k_r$.

The diffusion length is, hence, a function of nonradiative losses that can be quantified by measurement of the fluorescence quantum yield, Φ_F, shown in Figure 3b. The larger grain size results in an increased fluorescent yield. Data in Figure 4a follow the functional form of Equation 1, where the prefactor (R_{00}) is found to be 2.8 ± 0.2 nm, in agreement with $R_{00} = 3.3 \pm 0.3$ nm from Förster theory.[22] Fitting the diffusion length as a function of the measured grain size using Equation 3 yields $K_1 = 8 \pm 2$ and $K_2 = 7 \pm 2 \times 10^4$, as shown by the solid line in Figure 4b. The magnitude of K_2 is a function of quenching at grain boundaries, and therefore, determines the influence of crystalline grain size on L_D. A striking conclusion from this analysis is that the quenching rate at grain boundaries is found to be $\sim 10^4$ times larger than other nonradiative losses in single crystals (i.e., $K_2/K_1 = S_r/k_{nr}^0 \sim 10^4$). Since the diffusion lengths in the $[20\bar{1}]$ and [010] directions are likely to be smaller than in the [102] direction due to crystalline anisotropies (which is consistent with observations of charge mobility in PTCDA[1]), this suggests that the value for K_2 is likely a lower-limit estimate. However, given that exciton diffusion is a random process that samples all crystalline directions at each intermolecular hop, we do not anticipate such large anisotropies as in the case of drift mobility.[23] Furthermore, it is apparent from Figure 4 that a grain diameter $>20 \cdot (L_D$ for single crystals) no longer exhibits the effects of quenching at boundaries. Conceptually, this large critical grain diameter results from the large quenching velocity (proportional to K_2) that establishes a concentration gradient throughout the grain that draws in surrounding excitons.

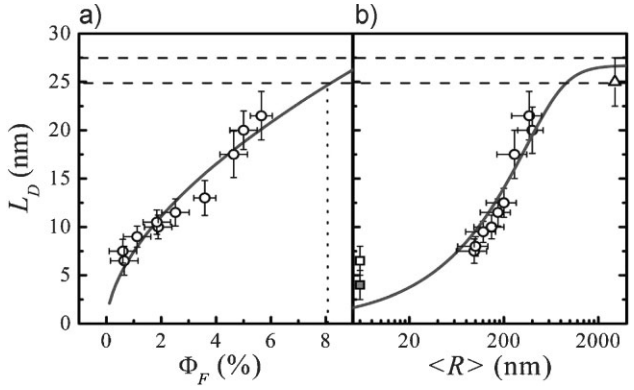

Figure 4. Measured exciton diffusion length (L_D) versus a) fluorescence quantum yield (Φ_F) and b) mean crystal diameter ($\langle R\rangle$). In (a), L_D is fit (line) with Equation 1, giving $R_{00} = 2.8$ nm for an interplanar molecular spacing of 0.32 nm, in agreement with the theoretical value of 3.2 nm. b) Data are iteratively fit (line) to Equation 3 giving $K_1 = 8 \pm 2$ and $K_2 = 7 \pm 2 \times 10^4$. Hollow circles correspond to measurements for crystalline films, hollow squares for amorphous films, filled squares to the diffusion length estimated from the measured quantum yield in (a) with Equation 1 ($\langle\kappa\rangle = 0.69$, $\langle a\rangle = 0.5$nm), and hollow triangles to the estimated diffusion length from the measured quantum yield limit in (a) for PTCDA single crystals. The single-crystalline limit is indicated by dashed lines. The diffusion length varies as a function of grain size due to nonradiative quenching at grain boundaries.

Since the enhancement in L_D with increasing crystalline order stems from reductions in nonradiative losses, material systems that have photoluminescence quantum yields approaching unity, such as anthracene,[27] should have little dependence on the crystal grain size. Regardless, very few materials actually exhibit such high quantum yields, particularly in neat films. Many organic materials employed in organic photovoltaic heterojunctions, including pentacene, tetracene, C_{60}, boron subphthalocyanine, chloroaluminum phthalocyanine, and copper phthalocyanine, have quantum mechanically allowed nonradiative transitions that result in low photoluminescence quantum yields, and therefore, are likely to show a strong dependence of L_D on $\langle R\rangle$. Other material systems, such as 1,4-bis(2-methylstyryl)benzene (*o*-MSB),[30] 1,4-bis(4-methylstyryl)-benzene (*p*-MSB),[30] *N,N′*-diphenyl-*N,N′*-bis(1-naphthyl)-1,1′-biphenyl-4,4″-diamine (NPD)[31] and tris(8-hydroxyquinolinato)-aluminum(III) (Alq_3),[32] which exhibit an increase in Φ_F with increasing crystalline order will likely have similarly enhanced diffusion lengths (c.f. Eq. 1). Note that PTCDA exhibits pronounced concentration quenching as demonstrated by a large difference between the single-crystal yield of $\Phi_F < 10\%$ and the solution-phase quantum yield of $\sim 50\%$.[33] This indicates that even in the presence of neat-film concentration quenching, other nonradiative losses can still be reduced by increasing the extent of crystalline order.

Nonradiative losses can also be introduced by impurities or dopants.[34] Oxygen incorporation, for example, can dramatically reduce the phosphorescent quantum yield in triplet emitting materials,[35] and therefore reduce L_D. The impact of such effects on the diffusion length remains to be explored.

In summary, we have shown that the exciton diffusion length in the archetypal organic semiconductor, PTCDA, is increased nearly fourfold over that of amorphous thin films through an increase in the extent of crystalline order. Diffusion is, in part, limited by nonradiative losses at grain boundaries, which are quantitatively measured via the magnitude of the radiative quantum yield as a function of grain size. This implies that systems where the quantum yield approaches unity are unlikely to show a dependence of the exciton diffusion length on crystalline order beyond the amorphous–polycrystalline transition. A simple model for grain boundary quenching combined with Förster-mediated singlet transport indicates that a PTCDA grain diameter of approximately 1 μm results in a diffusion length approximately equal to that of single-crystalline thin films. These results might lead to substantial efficiency enhancements in a wide range of excitonic organic electronic devices.

Experimental

PTCDA was obtained from Sigma-Aldrich and purified three times by thermal gradient sublimation [1]. Small (0.5 mm × 0.5 mm) single crystals of PTCDA were used for measurement of the single-crystal fluorescence

quantum yield. Films of PTCDA were grown in either a vacuum thermal evaporator (VTE) at a base pressure of $<10^{-6}$ Torr (1 Torr = 133.32 Pa), or by organic vapor-phase deposition [36] (OVPD) at 10 mTorr with a deposition rate of 0.4–0.5 nm s^{-1} and total thickness of 350 nm onto freshly cleaved KBr single-crystal substrates. Grain size was varied during the growth by controlling the substrate temperature (in VTE from 250–450 K, and in OVPD at 77 K). Additionally, thin (0.5 nm) templating layers of Ag were predeposited to hinder subsequent PTCDA crystallization, particularly for the amorphous samples grown by OVPD. Exciton blocking and quenching layers comprising 1,4,5,8-naphthalene-tetracarboxylic-dianhydride (NTCDA) (7.5 nm) and C_{60} (7.5 nm), respectively, were then deposited on the PTCDA films.

Spectrally resolved photoluminescence quenching (SR-PLQ) [22] measurements were carried out in a PTI spectrofluorometer at 45° incident and detection angles (relative to the substrate normal) under flowing nitrogen (see Supporting Information, Fig. S1 for a schematic of the experimental configuration). Excitation spectra of the PTCDA films with NTCDA and C_{60} blocking and quenching layers were collected between wavelengths of $\lambda = 350$ and 600 nm at the peak emission wavelength of 700 nm. A $\lambda = 500$ nm long pass filter was used at the monochromator exit port to avoid detecting higher-order reflections. An exciton blocking layer was found to be necessary to avoid quenching at the free PTCDA surface, consistent with the observation of grain-boundary quenching. The quenching ratio, η, is calculated as the ratio of the excitation spectrum intensity for the sample with the blocking layer to that of an equivalent sample with a quenching layer, corrected for transmission losses and reflection variations of the blocking and quenching layers. Since Förster transfer to the quenching layer is negligible for the materials used [22], $\eta = \alpha' L_D + 1$, from which we extract L_D, where the diffusion length has been defined as $L_D = \sqrt{D\tau}$. Transmission, reflection, and absorption coefficients were measured using a spectrophotometer. The error bars on the diffusion length were propagated from the uncertainty in the PL detection (i.e., multiple scans) for each sample, uncertainty in the absorption coefficient and from the error-weighted least squares fitting. The degree of quenching at the quenching interface was analyzed (see Supporting Information, Fig. S2) and found to be 97 ± 8% over the range of grain sizes. The uncertainty introduced into the exciton diffusion length by incomplete quenching is therefore ~8%, which is within the reported error.

Fluorescence quantum yields, Φ_F, of PTCDA films were measured in an integrating sphere (Labsphere) using a $\lambda = 475$ nm laser diode (intensity $\sim 10^{18}$ photon/cm^2 s) as the excitation source. The yields were calculated according to $\Phi_F = \int \frac{\lambda}{\hbar c} I_{Em} d\lambda / \int \frac{\lambda}{\hbar c} [I_B^L - I_F^L] d\lambda$ where $\hbar$ is Plank's constant divided by 2π, c is the speed of light, I_{Em} is the luminescence intensity from the film, I_B^L is the laser intensity from a bare substrate, and I_F^L is the background laser intensity reflected from the film [37]. The critical threshold for singlet–singlet annihilation in PTCDA is approximately $\sim 5 \times 10^{21}$ photon/cm^2 s [29], which is well above the incident flux used. The magnitudes of the measured Φ_F are within error of previous measurements for PTCDA [38]. Both the spectrometer and integrating sphere were calibrated using a tungsten-halogen lamp.

Crystal structure and orientation were examined with a rotating anode Rigaku Cu-Kα X-ray diffractometer (XRD) in the Bragg–Brentano configuration. Morphology, root-mean-square roughness, and grain size were investigated using a Nanoscope III Atomic Force Microscope (AFM) in the noncontact mode. Average crystal grain size was determined from AFM images through the Nanoscope III v3.5 software. Cross-sectional scanning electron microscopy (SEM) was used to correlate the AFM morphology to the underlying grain structure. Cleaved samples were coated with 5 nm Au to prevent charging in the SEM.

Acknowledgements

The authors thank the Department of Energy EERE Program, the Air Force Office of Scientific Research, and Global Photonic Energy Corp. for their support of this work. Additionally, the authors thank S. Kena-Cohen and N. C. Giebink for useful discussions. Supporting Information is available online from Wiley InterScience or from the author.

Received: August 17, 2009
Published online: December 1, 2009

[1] S. R. Forrest, *Chem. Rev.* **1997**, *97*, 1793.
[2] P. Peumans, A. Yakimov, S. R. Forrest, *J. Appl. Phys.* **2004**, *95*, 2938.
[3] J. G. Xue, B. P. Rand, S. Uchida, S. R. Forrest, *J. Appl. Phys.* **2005**, *98*, 124902.
[4] Y. R. Sun, N. C. Giebink, H. Kanno, B. W. Ma, M. E. Thompson, S. R. Forrest, *Nature* **2006**, *440*, 908.
[5] N. Karl, *Synth. Met.* **2003**, *133*, 649.
[6] S. R. Forrest, M. L. Kaplan, P. H. Schmidt, *J. Appl. Phys.* **1984**, *56*, 543.
[7] M. Shtein, J. Mapel, J. B. Benziger, S. R. Forrest, *Appl. Phys. Lett.* **2002**, *81*, 268.
[8] R. W. I. de Boer, M. E. Gershenson, A. F. Morpurgo, V. Podzorov, *Phys. Status Solidi A* **2004**, *201*, 1302.
[9] S. B. Rim, R. F. Fink, J. C. Schoneboom, P. Erk, P. Peumans, *Appl. Phys. Lett.* **2007**, *91*, 173504.
[10] Y. Terao, H. Sasabe, C. Adachi, *Appl. Phys. Lett.* **2007**, *90*, 103515.
[11] J. Kalinowski, *Organic Light-Emitting Diodes: Principles, Characteristics, and Processes*, Marcel Dekker, New York, NY **2005**.
[12] *Organic Electronic Materials: Conjugated Polymers and Low Molecular Weight Organic Solids* (Eds: R. Farchioni, G. Grosso), Springer, Berlin **2001**, Ch. 11.
[13] W. Hofberger, H. Bassler, *Phys. Status Solidi B* **1975**, *69*, 725.
[14] J. B. Aladekomo, S. Arnold, M. Pope, *Phys. Status Solidi B* **1977**, *80*, 333.
[15] R. R. Alfano, S. L. Shapiro, M. Pope, *Opt. Commun.* **1973**, *9*, 388.
[16] J. Kalinowski, *J. Lumin.* **1976**, *11*, 393.
[17] G. Vaubel, H. Kallmann, *Phys. Status Solidi* **1969**, *35*, 789.
[18] L. D. A. Siebbeles, A. Huijser, T. J. Savenije, *J. Mater. Chem.* **2009**, *19*, 6067.
[19] B. A. Gregg, J. Sprague, M. W. Peterson, *J. Phys. Chem. B* **1997**, *101*, 5362.
[20] D. E. Markov, C. Tanase, P. W. M. Blom, J. Wildeman, *Phys. Rev. B* **2005**, *72*, 045217.
[21] L. Pautmeier, B. Ries, R. Richert, H. Bassler, *Chem. Phys. Lett.* **1988**, *143*, 459.
[22] R. R. Lunt, N. C. Giebink, A. A. Belak, J. B. Benziger, S. R. Forrest, *J. Appl. Phys.* **2009**, *105*, 053711.
[23] R. C. Powell, Z. G. Soos, *J. Lumin.* **1975**, *11*, 1.
[24] B. J. Mulder, *Philips Res. Rep.* **1967**, *22*, 142.
[25] G. Vaubel, H. Baessler, *Mol. Cryst. Liq. Cryst.* **1970**, *12*, 47.
[26] T. Forster, *Discuss. Faraday Soc.* **1959**, *7*.
[27] M. Pope, C. E. Swenberg, *Electronic Processes in Organic Crystals and Polymers*, Oxford University Press, New York, NY **1982**.
[28] $a = 0.32$ nm in the [102] direction and 0.5 nm in the amorphous limit.
[29] E. Engel, K. Leo, M. Hoffmann, *Chem. Phys.* **2006**, *325*, 170.
[30] R. Kabe, H. Nakanotani, T. Sakanoue, M. Yahiro, C. Adachi, *Adv. Mater.* **2009**, *21*, 1.
[31] K. A. Osipov, V. N. Pavlovskii, E. V. Lutsenko, A. L. Gurskii, G. P. Yablonskii, S. Hartmann, A. Janssen, H. H. Johannes, R. Caspary, W. Kowalsky, N. Meyer, A. Gersdorff, A. Heuken, P. van Gemmern, C. Zimmermann, F. Jessen, H. Kalisch, R. H. Jansen, *Thin Solid Films* **2007**, *515*, 4834.
[32] V. V. N. R. Kishore, K. L. Narasimhan, N. Periasamy, *Phys. Chem. Chem. Phys.* **2003**, *5*, 1386.
[33] Z. G. Soos, M. H. Hennessy, V. Bulovic, *MRS Proc.* **2000**, 598.
[34] D. Donati, J. O. Williams, *Mol. Cryst. Liq. Cryst.* **1978**, *44*, 23.
[35] T. S. Yeh, C. S. Chu, Y. L. Lo, *Sens. Actuators B* **2006**, *119*, 701.
[36] M. Shtein, H. F. Gossenberger, J. B. Benziger, S. R. Forrest, *J. Appl. Phys.* **2001**, *89*, 1470.
[37] Y. Kawamura, H. Sasabe, C. Adachi, *Jpn. J. Appl. Phys. Part 1*, **2005**, *44*, 1160.
[38] A. Nollau, M. Hoffmann, K. Floreck, T. Fritz, K. Leo, *J. Appl. Phys.* **2000**, *87*, 7802.